PLASMA DYNAMICS

XIV. PLASMAS AND CONTROLLED NUCLEAR FUSION*

A. Waves and Radiation

Academic and Research Staff

Prof. G. Bekefi	Prof. B. Coppi	Dr. D. J. Sigmar
Prof. W. P. Allis	Prof. E. V. George	Dr. A. Treves
Prof. A. Bers	Dr. R. Gajewski	J. J. McCarthy
Prof. S. C. Brown	Dr. P. A. Politzer	W. J. Mulligan

Graduate Students

R. J. Becker	I. Inove	L. P. Mix, Jr.
H. Bhattacharya	L. Litzenberger	M. L. Vianna

RESEARCH OBJECTIVES

The major goal of this group is to generate a basic understanding of various types of oscillations and waves in ionized gases that are relevant to problems in thermonuclear fusion and space research.

1. Investigations of electromagnetic radiation emitted spontaneously by the plasma, because of thermal and nonthermal fluctuations of the free charges. At present, particular attention is being paid to emission generated as a result of many-body (collective) interactions between the charges at frequencies near the electron plasma frequency.

2. Studies of the dispersion characteristics of small-amplitude stable and unstable waves. We are now looking at the properties of ion sound waves in a facility that generates a collisionless plasma.

3. Investigation of nonlinear plasma phenomena is one of our major goals for the next few years. In this connection, we are particularly interested in the properties of large-amplitude waves, particle trapping, nonlinear Landau damping, parametric coupling of three or more waves, coupling of waves with particles, and turbulence.

4. Studies of fluctuation, particle losses, and turbulence in magnetic multipole geometries. For this purpose, we are constructing a steady-state linear quadrupole (SLIM-1). This is operated in the Francis Bitter National Magnet Laboratory.

G. Bekefi

1. LINEAR AND NONLINEAR RESPONSE OF A PLASMA SHEATH TO RF POTENTIALS

A plasma inherently is a highly nonlinear medium, and its nonlinear oscillatory behavior is being subjected to intense studies. These studies are concerned with interactions among different types of waves and between waves and charged particles

*This work was supported by the U.S. Atomic Energy Commission (Contract AT(30-1)-3980).

of the system. The main concern is with phenomena that exist in the bulk of the plasma; the plasma sheath, which necessarily separates any plasma from its external surroundings, has received relatively little attention. The main purpose of this report is to bring out the role of the plasma sheath as another important nonlinear element and to obtain better understanding of its characteristics. This work has been reported previously.[1-4] In this report we present our final conclusions.

A prerequisite to the understanding of the nonlinear response of any system is a knowledge of its linear characteristics. Thus, after briefly discussing the experimental apparatus we shall discuss the linear response of our system. The second part of this report is devoted to a study of the nonlinear response of our system.

Experimental Apparatus

The plasma sheath under investigation is in the form of a spherical shell surrounding a spherical metal probe inserted in a plasma. Figure XIV-1 is a schematic drawing of the experimental arrangement. The probe consists of two metal hemispheres separated by a narrow gap and is capable of being driven in antiphase by a voltage generator. The balun (General Radio 874-UBL) interposed between the generator and the probe

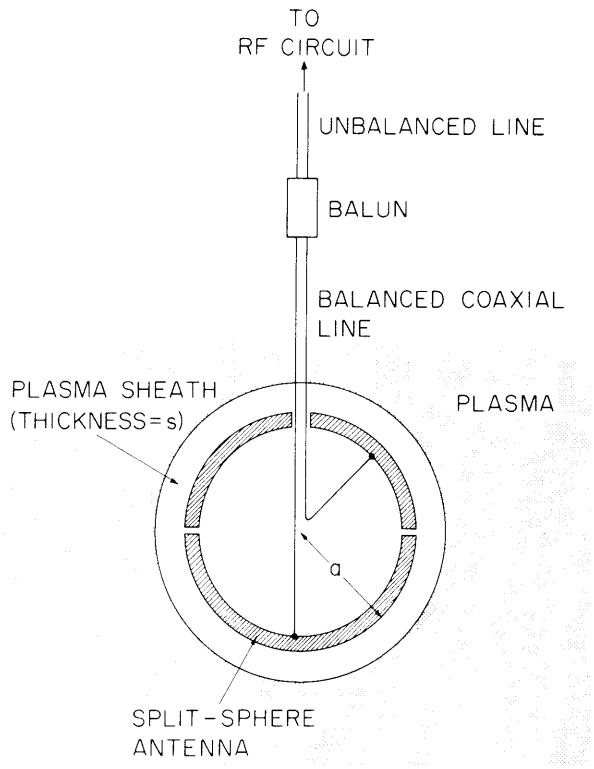

Fig. XIV-1. Experimental arrangement.

insures that no unbalanced RF currents flow to the probe and that the voltages on the two hemispheres are equal and opposite (about a common ground). We have studied the operation of such a "split-sphere antenna" in air by exploring its electric field configuration; we find that the electric fields are indeed predominantly dipolar, with some contribution from the next odd multipole also present.

In the experiments, antennas of various radii ranging from 1.6 cm to 3.8 cm are immersed in the plasma and driven with voltages ~0.5 V at frequencies between 50 MHz and 250 MHz. Except when stated otherwise, the metal hemispheres are insulated electrically from the plasma by a thin ($\sim 5\times10^{-3}$ cm) dielectric coating; thus no direct current flows and, in the absence of the RF voltage, the hemispheres are at the plasma floating potential.

The production, maintenance and characteristics of the plasma have been described in previous quarterly reports. Suffice it to note that the electron densities are typically 10^{8}-$10^{9}/cm^{3}$, the electron temperature in 3.4 eV, and the gas pressure is so low ($\sim 5\times10^{-4}$ Torr) that the plasma may be considered collisionless.

Linear Response

The most convenient way to describe and measure the linear RF current-voltage characteristics of our sheath-plasma system is in terms of its complex admittance Y, that is, the ratio of the current through the circuit to the voltage across its terminals. It is this admittance with which we are now concerned.

(a) Theoretical Model

The relevant dimensions of our plasma-antenna system are very small compared with the wavelength, and thus we are justified in computing the electric fields in the sheath and in the plasma from the quasi-static approximation. That is, we solve Laplace's equation in spherical coordinates, subject to the usual boundary conditions at the sheath-plasma boundary and at the surface of the antenna. In this manner, we derive the electric fields and, in particular, the radial electric field E_r at the surface (r=a) of the antenna in terms of the applied voltage V and the dielectric coefficient K.

The complex admittance Y = I/V may now be derived if we note that the current I flowing out of one hemisphere and entering the other is given by

$$I = j\omega\epsilon_o \int_0^{\pi/2} E_r(a)\, 2\pi^2 \sin\theta \, d\theta, \tag{1}$$

where $2\pi a^2 \sin\theta \, d\theta$ is an element of the antenna surface area. The result for Y is

$$Y = -j2\pi\epsilon_o \omega a \sum_{\ell=1,3,\ldots} F_\ell \left[\ell - \frac{2\ell+1}{Q_\ell}\right] \tag{2}$$

We have defined the Q_ℓ in a previous report[5] in which it was shown that admittance resonances exist when $Q_\ell \to 0$ and the admittance approaches zero when $Q_\ell \to (2\ell+1)/\ell$. The coefficient F_ℓ is related to the integral of the Legendre polynomial of order ℓ. It does not generate poles or zeros of the admittance.

The admittance given by Eq. 2 is amenable to a very useful and rather elegant interpretation in terms of lumped-circuit elements and we shall make much use of such a formalism. This is shown in Fig. XIV-2 where C is the capacitance of the vacuum sheath, and C_p, L_p, and R_p, are the capacitance, inductance, and resistance associated with the bulk of the plasma. A somewhat lengthy manipulation of Eq. 4 allows us to compute the actual values of these circuit elements. Assuming that the damping is light, we find that, for a given multipole ℓ,

$$C(\ell) \approx (a/s)\, H_\ell \tag{3a}$$

$$C_p(\ell) = (\ell+1)\, H_\ell \tag{3b}$$

$$L_p(\ell) \approx \left[(\ell+1)\omega_p^2 H_\ell\right]^{-1} \tag{3c}$$

$$R(\ell) \approx \left[(\ell+1)\omega_p H_\ell\right]^{-1} (\nu/\omega_p), \tag{3d}$$

where a is the probe radius, s is the sheath thickness, H_ℓ is $2\pi\epsilon_o a F_\ell$, and ν is some loss rate that can be due either to collisions or collisionless damping. These approximate equations are valid when s is much less than a; this is the case in all

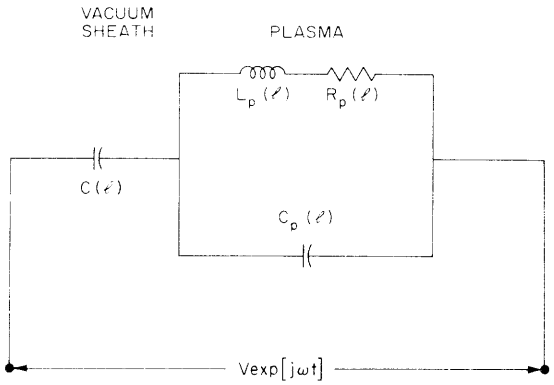

Fig. XIV-2. Lumped-circuit model.

of our experiments.

On the basis of Fig. XIV-2 and Eqs. 3, we see that the admittance exhibits series resonances at frequencies $\omega = \omega_R = [C(\ell)L_p(\ell)]^{-1/2}$. Substituting for $C(\ell)$ and $L(\ell)$ from Eqs. 3a and 3c, we obtain

$$(\omega_R/\omega_p) \approx [(\ell+1)(s/a)]^{1/2} \tag{4}$$

Likewise, "antiresonances" occur when $\omega = \omega_A = [C_p(\ell)L_p(\ell)]^{-1/2}$, and these are given by

$$(\omega_A/\omega_p) \approx 1. \tag{5}$$

(b) Observations

The RF admittance measurements are carried out by attaching an RF admittance bridge (General Radio 1602B) to the unbalanced section of coaxial line shown in Fig. XIV-1. The measurements are made 130 cm from the split-sphere antenna. The results must be transformed by means of the usual transmission-line equations to obtain the admittance <u>at</u> the terminals of the antenna. Also, the "stray" reactances associated with internal capacitance of the hollow hemispheres and the inductance associated with the wire leads inside the hemispheres must be removed. These two circuit elements are deduced from admittance measurements made in free space. Only after making the various transformations are we justified in making comparisons with the theory outlined above. Henceforth, all results shown refer to admittances that have been transformed appropriately.

Figure XIV-3 illustrates typical measurements made with an antenna of 3.8 cm radius. The solid points refer to the conductance, the open circles to the susceptance [i.e., the real and imaginary parts of $Y(\omega)$]. We observe two resonances, a strong one at 56 MHz, and a weaker one at 78 MHz. A blown-up view of the weaker one (after subtraction of the contributions from the stronger one) is shown in the lower figure. These two resonances are, respectively, the dipole (ℓ=1) and the next higher multipole (ℓ=3) contributions to $Y(\omega)$.

At and near a given resonance ℓ, the sheath capacitance $C(\ell)$, the plasma inductance $L_p(\ell)$ and the plasma resistance $R_p(\ell)$ are the principal circuit elements that contribute to the resonant behavior; the plasma capacitance $C_p(\ell)$ of fig. XIV-2 contributes weakly. Thus the admittance Y is approximately given by

$$Y(\ell) = \frac{R_p(\ell)}{R_p(\ell) + j[\omega L_p(\ell) - (\omega C(\ell))^{-1}]}, \tag{6}$$

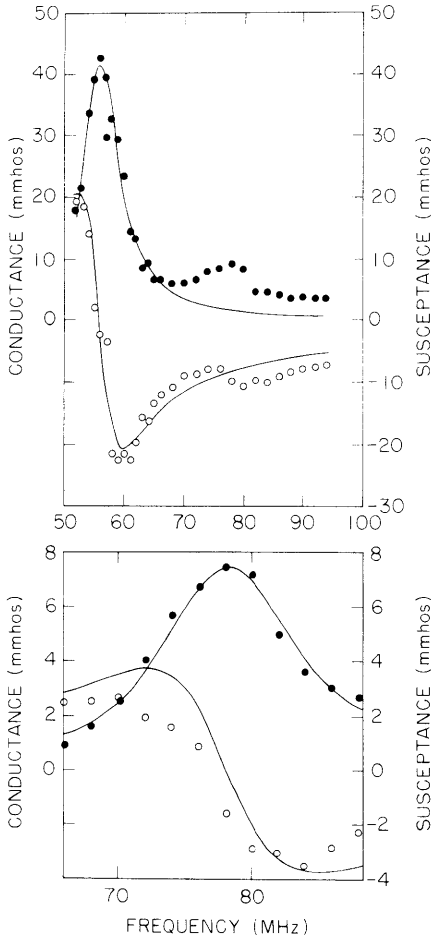

Fig. XIV-3.

(a) Admittance vs frequency for antenna of 3.8 cm radius.
(b) Octupole ($\ell = 3$) admittance. Solid points, conductance; open circles, susceptance; solid line, series circuit fit.

Table XIV-1. Values of measured circuit elements obtained by fitting the experimental points of Fig. XIV-3 to Eq. 6.

	$\ell = 1$	$\ell = 3$
$\omega_R/2\pi$	56 MHz	78 MHz
$R_p(\ell)$	24 Ω	133 Ω
$L_p(\ell)$	0.50×10^{-6} H	1.70×10^{-6} H
$C(\ell)$	16.1×10^{-12} F	2.46×10^{-12} F

and the circuit elements can be evaluated by fitting this equation to the experimental results. The solid lines of Fig. XIV-3 represent the best fit obtainable, Table XIV-1 gives the values of $C(\ell)$, $R_p(\ell)$, and $L_p(\ell)$ thus obtained. We may now, even without knowledge of ω_p and the sheath thickness s, examine the extent to which theory agrees with the experimental values. Taking the ratio $\omega_R(1)/\omega_R(3)$ from Table XIV-1 yields $\omega_R(1)/\omega_R(3) = 0.718$ and Eq. 4 gives 0.707. Similarly, Table XIV-1 gives $C(1)/C(3) = 6.55$ and Eq. 3a gives 6.85. This good agreement lends support to the validity of the theoretical model.

Once the sheath capacitance $C(\ell)$ is determined experimentally as described above, use of Eq. 3a immediately yields the effective sheath thickness s. Since we may expect s to vary linearly with Debye length $L_D = [\epsilon_o KT/Ne^2]^{1/2}$, it is convenient to write $s = pL_D$ and determine the numerical coefficient p. We have determined $C(1)$ for antennas of 3 different radii [a = 1.6, 2.2, and 3.8 cm] and for several different values of electron density N. Figure XIV-4 shows the experimental results, together with the theoretical curve obtained from Eq. 3a for the case $s = 3.3L_D$. This value of sheath thickness agrees well with earlier estimates.[6] Using it in the exact form of Eq. 4 tells how the resonant frequency ω_r varies with a/L_D. This is shown as the solid line in Fig. XIV-5, together with the experimental points.

We realize that the theoretical model of a perfectly uniform plasma surrounding a vacuum sheath devoid of charges is but a first crude approximation to the physical situation. Buckley,[7] and DeAngelis and Baldwin[8] consider more refined models. Buckley calculates radial electron trajectories around a spherical monopole (ℓ=0) probe; DeAngelis and Baldwin make allowance for the expected density gradients that must exist in the boundary separating the plasma bulk from the sheath. The calculations of DeAngelis and Baldwin are shown in Fig. XIV-5 by the dashed line. The good agreement gives us added confidence in the vacuum-sheath model.

We also wish to point out the relevance of these results to plasma diagnostics. Equation 5 shows that the antiresonance frequency is very insensitive to the precise value of the sheath thickness and therefore a determination of ω_A could, in principle, be used as a diagnostic tool to determine the plasma frequency. Unfortunately, because of heavy damping, the antiresonance is usually poorly defined and often is not even observed in the experiments. When it is observed, the admittance in its vicinity varies so slowly with frequency that large errors are easily made in determining the crossover point where the admittance changes sign. On the other hand, we cannot use the resonance frequency in the determination of ω_p (Eq. 4) unless the sheath thickness s is known or is determined by some other means. This has been the difficulty in most previous experiments. Our method of fitting a series RLC circuit to the admittance results gave us experimental values to plug into Eq. 3a. This is our independent determination of s which can now be used to determine ω_p unambiguously.

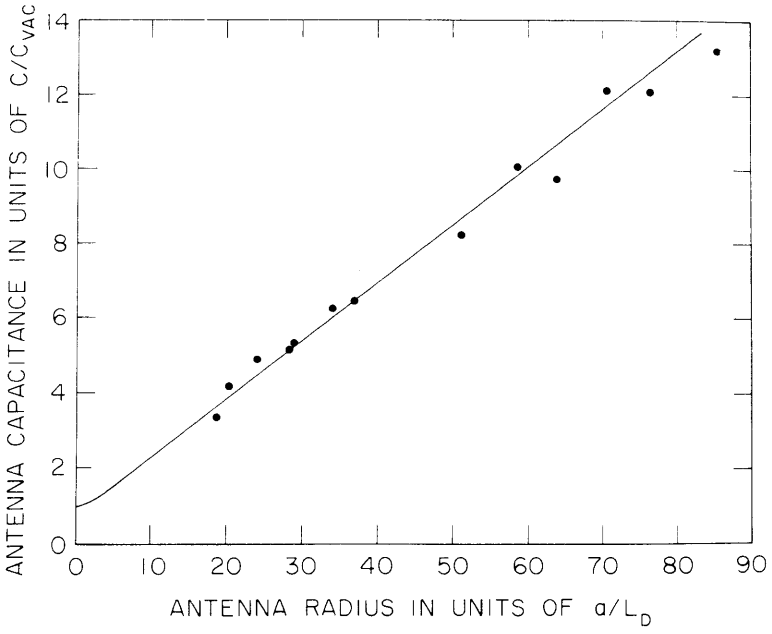

Fig. XIV-4. Sheath capacitance vs antenna radius. Solid points, experiment; solid line, theory.

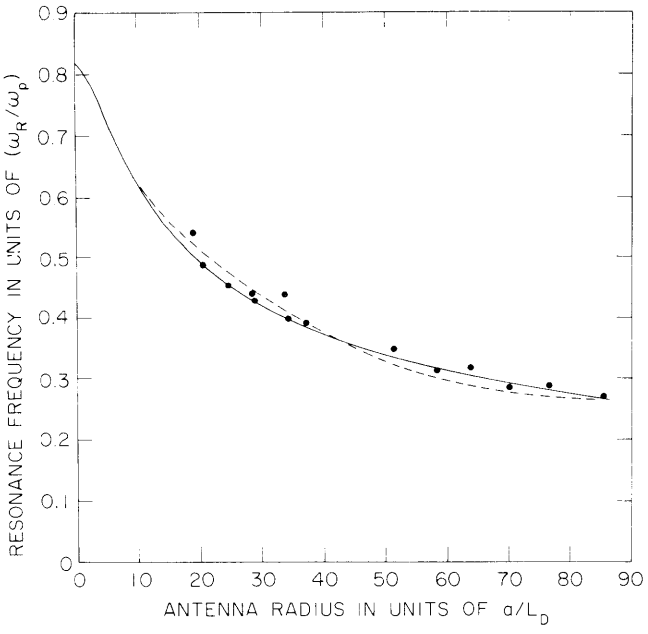

Fig. XIV-5. Series resonance frequency vs antenna radius. Solid points, experiment; solid line, vacuum sheath theory; dashed line, DeAngelis and Baldwin theory.

Nonlinear Response

To observe the nonlinear response of our sheath-plasma system we send a sinusoidal signal down the transmission line to our split-sphere antenna and observe the generation of harmonic signals in the reflected wave. The experimental details have been discussed in a previous report.[3] We shall show that the amplitude of these harmonics relative to the amplitude of the imposed RF voltage can be fully explained by the following simple model. The oscillating field causes a sinusoidal motion of the electrons in the boundary separating the vacuum sheath from the bulk of the plasma. This motion causes the vacuum-sheath capacitance of Eq. 3a to have a time-variant component. This time-variant capacitance is the nonlinear element that we seek.

(a) Theoretical Model

Instead of assuming that the electric field at the probe surface is sinusoidal, as we did in deriving Eq. 1 for the linear case, we let E be a still unspecified function of time. The general form of Eq. 1 is

$$I(t) = \epsilon_o \int \frac{d\vec{E}_r(t)}{dt} \cdot d\vec{A} \qquad (r=a). \tag{7}$$

By writing E(t) in terms of the applied potential V(t) and a factor P(t) which depends on the terms $\ell - \frac{2\ell + 1}{Q_\ell}$ of Eq. 2, we obtain

$$I(t) = -\epsilon_o \frac{dV(t)}{dt} \int P \cdot dA - \epsilon_o V(t) \int \frac{dP}{ds} \frac{ds}{dt} \cdot dA. \tag{8}$$

The first term yields the linear admittance, while the second term, which varies in time because the sheath thickness s varies in time, yields the nonlinear results. After much algebraic manipulation, including substitution of values for Q_ℓ, we find, for the $\ell = 1$ multipole, that the nonlinear voltage generated across the antenna can be written

$$V_{N.L.}(t) = \frac{16}{9} \frac{1}{(\epsilon_o A)^2} \left(\frac{e}{m\omega_p^2}\right) \left(\int I(t)\, dt\right)^2, \tag{9}$$

where A is the surface area of a hemisphere.

To compute the amplitude of the harmonic signals, we must Fourier-analyze the current I(t) in the nonlinear term. Consider, for example, the second harmonic. The voltage from the external oscillator at a frequency ω drives a current at the same frequency through the sheath-plasma system. As we learned from the linear

characteristics, this current is determined by the linear impedance at that frequency ω. Since this current appears as the square in the nonlinear term, it will give rise to a voltage at the second harmonic which in turn drives the second-harmonic current. It is important to note that the flow of the second-harmonic current depends on the impedance at the second harmonic. Thus the measured harmonic output reflected back from the antenna critically depends not only on the plasma characteristics at the fundamental frequency but also on its properties at the second harmonic. Succeeding iteration processes lead to 3^{rd}, 4^{th} and 5^{th} harmonics, and so on.

Figure XIV-6 shows the results for the harmonics obtained with the antenna

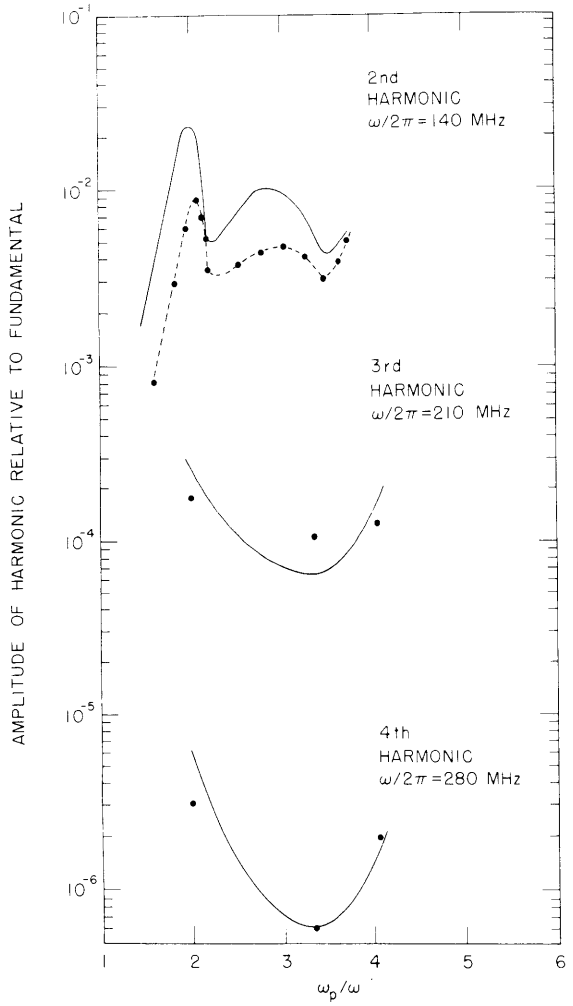

Fig. XIV-6. Harmonics vs ω_p/ω. Solid points, experiment; solid line, theory.
f_{inc} = 70 MHz.
V_{inc} = 0.5 V.

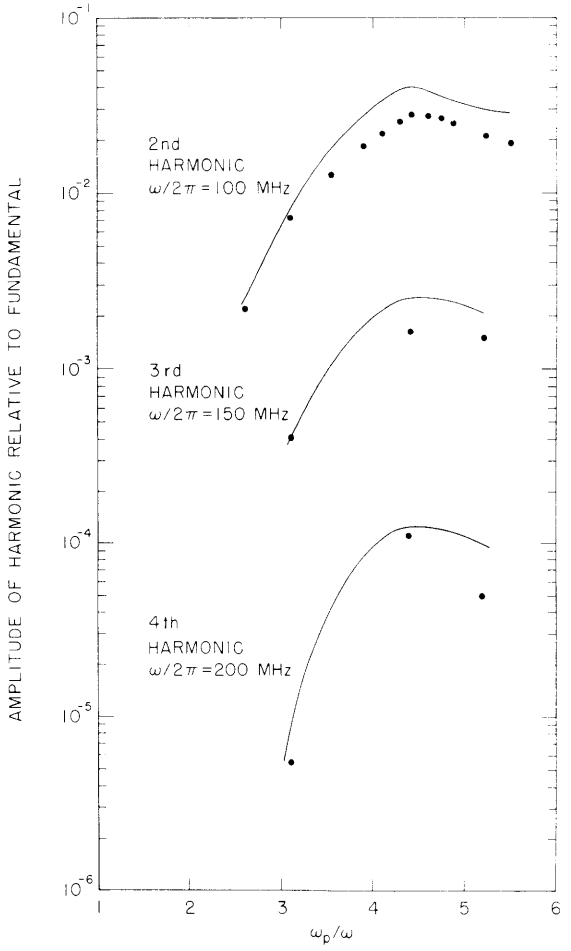

Fig. XIV-7. Harmonics vs ω_p/ω. Solid points, experiment; solid line, theory.
f_{inc} = 50 MHz.
V_{inc} = 0.5 V.

of 1.6 cm radius. The points are the experimental results for the first 3 harmonics and are joined with the dashed line. The solid lines are calculated from the nonlinear equations. In these measurements, the oscillator is held constant at a frequency of 70 MHz and the plasma density is varied. The vertical scale is the amplitude of the measured voltage relative to a fixed oscillator voltage of 0.5 V. The shape of the response reflects the resonance characteristics of the sheath-plasma system. When the ratio of plasma frequency to oscillator frequency coincides with a natural mode of oscillation, the harmonic output is enhanced. The harmonic falls off rapidly on both sides of the resonance. The detailed line shapes, showing, for example, the minima at the 3^{rd} and 4^{th} harmonics, are due entirely to the impedance characteristics at the 2^{nd} and higher harmonics.

The importance of these impedance characteristics at the higher harmonics is emphasized in Fig. XIV-7. Here we adjusted the frequency of the oscillator so that

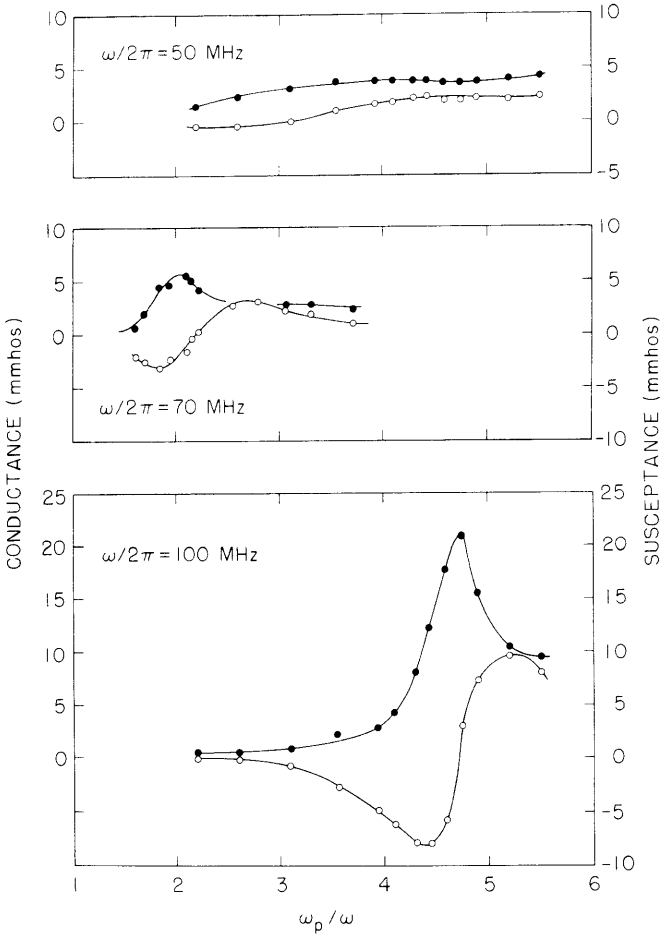

Fig. XIV-8. Admittance vs ω_p/ω for the conditions of Figs. XIV-6 and XIV-7. Solid points, conductance; open circles, susceptance.

the second harmonic (100 MHz), rather than the fundamental frequency (50 MHz), coincided with a natural mode of our system. Once again we see quite good agreement between experiment and theory. We should stress that in making these comparisons between measured and computed harmonic signals no adjustable parameters were introduced into the relevant nonlinear equations.

In Fig. XIV-8 we show the measured values of the admittances corresponding to the harmonic results of Fig. XIV-6 and XIV-7. In Fig. XIV-8b, we see the resonance that occurs at the fundamental frequency and enhances the harmonic output in Fig. XIV-6. In Fig. XIV-8a we see that the admittance at 50 MHz is devoid of resonances, and it is the admittance resonance at 100 MHz that enhances the harmonic output of Fig. XIV-7.

In conclusion, we have shown that the relatively simple model of an oscillating vacuum sheath very satisfactorily predicts the nonlinearities that might exist in many experiments whenever a plasma sheath is excited by RF oscillations. We have imposed voltages that are small compared with the voltage drop across the sheath, and thus the harmonic content is but a few per cent of the amplitude of the fundamental. Under strong driving conditions and in the neighborhood of natural modes of the coupled sheath-plasma system, harmonic generation will be a major effect.

A. J. Cohen, G. Bekefi

References

1. A. J. Cohen, Quarterly Progress Report No. 85, Research Laboratory of Electronics, M. I. T., April 15, 1967, pp. 103-107.
2. A. J. Cohen, Quarterly Progress Report No. 90, Research Laboratory of Electronics, M. I. T., July 15, 1968, pp. 76-82.
3. A. J. Cohen, Quarterly Progress Report No. 94, Research Laboratory of Electronics, M. I. T., July 15, 1969, pp. 108-121.
4. A. J. Cohen, Quarterly Progress Report No. 97, Research Laboratory of Electronics, M. I. T., April 15, 1970, pp. 45-46.
5. D. F. Smith and G. Bekefi, Quarterly Progress Report No. 74, Research Laboratory of Electronics, M. I. T., July 15, 1964, p. 91.
6. R. S. Harp and F. W. Crawford, J. Appl. Phys. 35, 3436 (1964).
7. R. Buckley, Proc. Roy. Soc. (London), Vol. 290A, pp. 186-219, 1966.
8. D. DeAngelis and D. Baldwin (Private communication).

2. NEW VIEWS ON THE SELF-CONSISTENT ELECTROSTATIC PROBLEM

Introduction

The study of the initial and boundary-value problems for electrostatic disturbances in a hot plasma using the Vlasov equation is still of considerable interest. Although it

is a very old problem, some important aspects are not well understood and some are even completely unknown. Among these we mention the case of an inhomogeneous plasma in the linearized approximation and the nonstationary nonlinear problem for a homogeneous medium. In these cases the usual Fourier-Laplace transform method cannot be applied, and this means that we should study the problems in a space-time language. As a natural start for the study of the nonlinear problem we should see what we can get in the linear case, and in this report the linear theory of electrostatic disturbances in a homogeneous plasma is reviewed from the point of view of a space-time description, and simple exact solutions of the initial and boundary-value problems are presented with a new way of deriving old results. The method consists in finding solutions to integral equations representing the initial and boundary-value problems.

Integral Equation for the Number Density-Initial Value Problem

Assume that we have found the initial perturbed distribution function $f_1(x, t=o, v)$ in all space. We want to find $f_1(x, t, v)$ and $E(x, t)$, given $f_o(v)$.

$$\frac{\partial f_1}{\partial t} + v \frac{\partial f_1}{\partial x} = \frac{en_o}{m} E(x,t) \frac{\partial f_o}{\partial v} \tag{1a}$$

$$\frac{\partial E}{\partial x} = -4\pi e \int_{-\infty}^{\infty} (dv)\, f_1 \tag{1b}$$

To integrate (1a) formally in time, apply the translation operator $e^{tv\,\partial/\partial x}$ to both sides ($f_1(x)$ is expandable in Taylor series). Then (1a) becomes

$$\frac{\partial}{\partial t}\left[e^{tv\,\partial/\partial x} f_1(x,t,v)\right] = \frac{en_o}{m} E(x+vt,t) \frac{\partial f_o}{\partial v}. \tag{2}$$

Integration between zero and t gives

$$e^{tv\,\partial/\partial x} f_1(x,t,v) - f_1(x,o,v) = \frac{en_o}{m} \frac{\partial f_o}{\partial v} \int_0^t E(x+vt', t')\, dt'. \tag{3}$$

Multiplying by the inverse operator, we get

$$f_1(x,t,v) = f_1(x-vt,o,v) + \frac{en_o}{m} \frac{\partial f_o}{\partial v} \int_0^t E[x-v(t-t'), t']\, dt'. \tag{4}$$

Equation 4 tells us that once the electric field $E(x,t)$ is known, we can immediately find $f_1(x,t,v)$. Now define $n(x,t)$, the relative number density, by

$\int_{-\infty}^{\infty}$ (dv) $f_1 = n(x,t)$, and integrate (4) in v. We may then write

$$n(x,t) = n_F(x,t) + \frac{en_o}{m} \int_{-\infty}^{\infty} dv \frac{\partial f_o}{\partial v} \int_0^t E[x - v(t-t'), t'] \, dt', \tag{5}$$

where $n_F(x,t) = \int_{-\infty}^{\infty} dv \, f_1(x - vt, o, v)$. We may now invert the order of integration in the double integral and integrate by parts.

$$\int_{-\infty}^{\infty} dv \frac{\partial f_o}{\partial v} E[x - v(t-t'), t'] = (t-t') \int_{-\infty}^{\infty} dv \, f_o(v) \; D_1 E[x - v(t-t'), t'], \tag{6}$$

where D_1 indicates derivative with respect to the first argument.

We may now introduce the variable x' in (6) by $v = \frac{x - x'}{t - t'}$. This gives

$$\int_{-\infty}^{\infty} dv \frac{\partial f_o}{\partial v} E[x - v(t-t'), t'] = \int_{-\infty}^{\infty} dx' \; f_o\left[\frac{x - x'}{t - t'}\right] \frac{\partial E}{\partial x'}(x', t'). \tag{7}$$

Then, making use of Poisson's equation (1b) and the definition of n(x,t), we get from (5), (6), and (7) the equation for n.

$$n(x,t) = n_F(x,t) - \omega_p^2 \int_0^t dt' \int_{-\infty}^{\infty} dx' \; f_o\left[\frac{x - x'}{t - t'}\right] n(x', t'), \tag{8a}$$

with

$$n_F(x,t) = \int_{-\infty}^{\infty} dv \, f_1(x - vt, o, v). \tag{8b}$$

Equations 8 have a simple physical interpretation. If the process were completely interactionless, only the first term would be sufficient to describe the time evolution. The second term reflects the effect of the long range interaction potentials and plays the role of a collective collision operator.

Once n(x,t) is determined, Poisson's equation gives us the electric field with which we may find $f_1(x,t,v)$ by use of Eq. 4.

Equation 8a has a unique solution, and standard techniques may be used to find it. The most powerful one is based on a successive approximation scheme.[1] We may write Eq. 8a as

$$n = n_F - \omega_p^2 f_o * n, \tag{9}$$

where the star operation denotes the two-dimensional convolution in (8a).

The solution is then given by

$$n = n_F - \omega_p^2 H * n_F, \tag{10}$$

where

$$H = \sum_{n=0}^{\infty} \left(-\omega_p^2\right)^n *^n f_o \tag{11}$$

and $*^o f_o = f_o$, $*^n f_o = \underbrace{f_o * f_o * \ldots * f_o}_{n \text{ stars}}$. In our specific case,

$$*^n f_o = \int_0^t dt_1 \ldots \int_0^{t_{n-1}} dt_n \int_{-\infty}^{\infty} dx_1 \ldots \int_{-\infty}^{\infty} dx_n \, f_o\left[\frac{x - x_1}{t - t_1}\right] f_o\left[\frac{x_1 - x_2}{t_1 - t_2}\right]$$

$$\ldots f_o\left[\frac{x_{n-1} - x_n}{t_{n-1} - t_n}\right] f_o\left[\frac{x_n}{t_n}\right]. \tag{12}$$

It is convenient to write the formula (12) for the Fourier-transformed problem in space. Equation 9 will then be a Volterra equation of second kind.[2] The Fourier transform of (12) is

$$F\left[*^n f_o\right] = (2\pi)^{n/2} \int_0^t dt_1 \ldots \int_0^{t_{n-1}} dt_n (t-t_1) \ldots (t_{n-1}-t_n) t_n \, F_o[k(t-t_1)]$$

$$\ldots F_o[k(t_{n-1}-t_n)] \, F_o(kt_n) \tag{13a}$$

and

$$F_o(k) = \frac{1}{\sqrt{2\pi}} \int_{-\infty}^{\infty} (dv) \, e^{-ikv} f_o(v) \tag{13b}$$

Had we Fourier-Laplace transformed Eq. 8a, we should have obtained Landau's formula

$$n(k, s) = \frac{1}{K_L(k, s)} \int_{-\infty}^{\infty} dv \, \frac{F_1(k, v)}{s + ikv} \tag{14a}$$

$$K_L(k, s) = 1 + \omega_p^2 \int_{-\infty}^{\infty} \frac{f_o(v)}{(s+ikv)^2} \, dv; \qquad \text{Re}(s) > 0, \tag{14b}$$

where F_1 is the Fourier transform of $f_1(x, o, v)$ in x.

Solution of the Initial-Value Problem

We shall now study the general properties of the resolvent Kernel (11). We may write it

$$H = \sum_{n=0}^{\infty} \left(-\omega_p^2\right)^n a_{n+1}(x,t), \tag{15}$$

with $a_{n+1}(x,t) = *^n f_o$. If we can find an operator T(x,t) that can act on (12) to give

$$T(x,t)\, a_{n+1}(x,t) = a_n(x,t), \tag{16}$$

or an operator T(k,t) that can act similarly on (13), we get from (15)

$$\left(T + \omega_p^2\right) H = 0 \tag{17}$$

which, together with some initial conditions, plays the role of a "resolvent" dispersion equation. The general properties of this equation will not be studied in this report, but two examples will be given using a resonance type of distribution functions. This method does not appear to have been used previously to solve this kind of equation.

The Lorentzian Distribution

We shall now study the problem with the Lorentzian equilibrium distribution function $f_o(v) = v_T/\pi\left(v_T^2 + v^2\right)$.

We chose to work with the Fourier transform of (8a):

$$n(k,t) = n_F(k,t) - \omega_p^2 \sqrt{2\pi} \int_0^t dt'\, (t-t')\, F_o[k(t-t')]\, n(k,t'), \tag{18}$$

where F_o is defined by (13a). In our case,

$$F_o(kt) = \frac{e^{-|kv_T t|}}{\sqrt{2\pi}},$$

and formulas (15) and (13) give

$$a_{n+1}(k,t) = e^{-kv_T t}\, b_{n+1}(t), \tag{19a}$$

where

$$b_{n+1}(t) = \int_0^t dt_1 \cdots \int_0^{t_{n-1}} dt_n\, (t-t_1) \cdots (t_{n-1}-t_n)\, t_n, \tag{19b}$$

and $b_1(t) = t$. It is seen that $b''_{n+1}(t) = b_n(t)$, so that, if we write (15) as

$$H = e^{-kv_T t}\, \phi(t); \qquad \phi(t) = \sum_{n=0}^{\infty} \left(-\omega_p^2\right)^n b_{n+1}(t), \tag{20}$$

we then have

$$\phi''(t) + \omega_p^2 \phi(t) = 0, \tag{21}$$

and the initial conditions are $\phi(o) = 0$ and $\phi'(o) = 1$. Then $\phi(t) = \frac{1}{\omega_p} \sin \omega_p t$ and the solution to (18) is[3]

$$n(k,t) = n_F(k,t) - \omega_p \int_0^t e^{-kv_T t'} \sin \omega_p t' n_F(k, t-t'). \tag{22a}$$

If we Fourier-invert this formula, we get

$$n(x,t) = n_F(x,t) - \omega_p \int_0^t \frac{dt'}{t-t'} \sin \omega_p (t-t') \int_{-\infty}^{\infty} dx'\, f_o\left[\frac{x-x'}{t-t'}\right] n_F(x', t'). \tag{22b}$$

If we have a standing wave as initial state, we may write

$$f_1(x, o, v) = \frac{2e v_T \phi_o}{m\pi} \frac{e^{-ikx}}{\left(v_T^2 + v^2\right)^2}, \tag{23}$$

where $\phi_o\, e^{-ikx}$ is the wave electric potential, and (22b) will give

$$n(x,t) = \frac{e\phi_o}{mV_T^2}\, e^{-ikx - kv_T t} \left(\cos \omega_p t + \frac{kv_T}{\omega_p} \sin \omega_p t\right). \tag{24}$$

It is peculiar to a Lorentzian distribution that there is no dispersion. Following the usual method, one would find[4] for the dispersion relation $\omega = \mp\omega_p - ikv_T$. Formula (24) also shows that the perturbation dies off with the Landau damping constant kv_T, oscillating with frequency ω_p.

Higher Resonance-Type Equilibrium Distributions

For $f_o(v) = \dfrac{2v_T^3/\pi}{\left(v_T^2 + v^2\right)^2}$, the dispersion relation gives a Bohm-Gross type of formula for long wavelengths and Landau damping. We shall only indicate the calculations that illustrate the way to find the resolvent equation, since we do not now study the features of the exact solutions.

In this case $F_o(kt) = (1+kv_T t)\, e^{-kv_T t}$. The equation analogous to (19b) is

$$b_{n+1}(t) = \int_0^t dt_1 \cdots \int_0^{t_{n-1}} dt_n\, (t-t_1)\left[1+kv_T(t-t_1)\right] \cdots t_n(1+kv_T t_n) \tag{25}$$

and $b_1(t) = t(1+kv_T t)$. To find the operator T for Eq. 17, we note that

$$b_n'''(t) = \left(\frac{\partial}{\partial t} + kv_T\right) b_{n-1}(t). \tag{26}$$

If we solve Eq. 26 formally for $b_{n-1}(t)$, we get

$$\int_0^t e^{-kv_T(t-t')}\, b_n'''(t')\, dt' = b_{n-1}(t) \tag{27}$$

which is equivalent to

$$b_n'' - kv_T b_n' + k^2 v_T^2 b_n - k^3 v_T^3 \int_0^t e^{-kv_T(t-t')}\, b_n(t')\, dt' = b_{n-1}(t), \tag{28}$$

and from this the equation analogous to (21) follows:

$$\phi'' - kv_T\phi' + \left(\omega_p^2 + k^2 v_T^2\right)\phi - k^3 v_T^3 \int_0^t dt'\, e^{-kv_T(t-t')}\, \phi(t') = 0. \tag{29}$$

This equation is easily soluble by the Laplace-transform method, and the solution may be obtained by Laplace-inverting the formula

$$L(\phi) = \frac{s + kv_T}{s^3 + \omega_p^2 s + \omega_p^2 kv_T} \tag{30}$$

which is obtained from the Laplace transform of (29). We do not write down the exact

formula for the resolvent kernel because it is messy and we are not interested in it right now.

Integral Equation for the Boundary-Value Problem

Assume we can find $f_1(x=o,t,v)$. Then, given f_o, we may Fourier-analyze the Vlasov-Poisson system in time and write

$$\frac{\partial f_1}{\partial x} + \frac{i\omega}{v} f_1 = \frac{en_o}{mv} E(x,\omega) \frac{\partial f_o}{\partial v} \tag{31a}$$

$$\frac{\partial E}{\partial x} = -4\pi e \int_{-\infty}^{\infty} (dv)\ f_1 \tag{31b}$$

Integrating (31a) between zero and x yields

$$f_1(x,\omega,v) = e^{-i\omega x/v} f_1(o,\omega,v) + \frac{en_o}{mv} \frac{\partial f_o}{\partial v} e^{-i\omega x/v} \int_0^x dx'\ e^{i\omega x'/v} E(x',\omega). \tag{32}$$

By integrating the last term by parts, Eq. 32 becomes

$$f_1(x,\omega,v) = e^{-i\omega x/v} f_1(o,\omega,v) + \frac{en_o}{i\omega m} \frac{\partial f_o}{\partial v} \left[E(x,\omega) - e^{-i\omega x/v} E(o,\omega) \right.$$

$$\left. - e^{-i\omega x/v} \int_0^x dx'\ e^{i\omega x'/v} \frac{\partial E}{\partial x'}(x',\omega) \right]. \tag{33}$$

Using (31b) in the last term and integrating (33) in v, and with $n(x,\omega) = \int (dv) f_1(x,\omega,v)$, we get

$$n(x,\omega) = n_L(x,\omega) + \frac{\omega_p^2}{i\omega} \int_0^x dx'\ n(x',\omega) \int_{-\infty}^{\infty} dv\ \frac{\partial f_o}{\partial v} e^{-\frac{i\omega}{v}(x-x')}, \tag{34a}$$

where

$$n_L(x,\omega) = \int_{-\infty}^{\infty} dv\, e^{-i\omega x/v} \left[f_1(o,\omega,v) - \frac{n_o e}{i\omega m} E(o,\omega) \frac{\partial f_o}{\partial v} \right]. \tag{34b}$$

In (34b) the $E(o,\omega)$, by virtue of Maxwell's equations, may be written

$$E(o,\omega) = \frac{4\pi e}{i\omega} \int_{-\infty}^{\infty} v f_1(o,\omega,v)\, dv. \tag{34c}$$

Again, (34a) is a convolution type of integral equation.

As an interesting example of these equations, we write down the solution for the Lorentzian distribution without the calculations that are completely symmetrical to the initial-value problem.

In this case, the equation analogous to (21) is

$$\phi''(x) - \left(\frac{\omega_p}{v_T}\right)\phi(x) = 0 \tag{35}$$

and

$$\phi(x) = \frac{v_T}{\omega_p}\sinh\left(\frac{\omega_p}{v_T}\right)x, \tag{36}$$

so that

$$n(x,\omega) = n_L(x,\omega) + \frac{\omega_p}{v_T}\int_0^x dx'\, e^{-\frac{\omega}{v_T}x'}\sinh\left(\frac{\omega_p}{v_T}x'\right) n_L(x-x',\omega), \tag{37}$$

or if we Fourier-invert (37),

$$n(x,t) = n_L(x,t) + \frac{\omega_p}{v_T}\int_0^x (dx')x'\sinh\left(\frac{\omega_p}{v_T}x'\right)\int_{-\infty}^{\infty}\frac{dt'}{t'^2} f_o\left(\frac{x'}{t'}\right) n_L(x-x', t-t'), \tag{38}$$

where f_o is the Lorentzian distribution. The effort is now being concentrated on the solution of these problems for a Maxwellian f_o. An equation formally equal to (8a) has been used recently by A. J. Turski[5] to investigate the time-asymptotic behavior of the resolvent kernel.

M. L. Vianna

References

1. F. G. Tricomi, Integral Equations (Interscience Publishers, Inc., New York, 1957), Chap. I.
2. See Eq. 18 below. It has been known since 1960; see O. Penrose, Phys. Fluids 3, 258 (1960).
3. J. Levin, Phys. Fluids 10, 1307 (1967).
4. R. J. Briggs, Electron-Stream Interaction with Plasmas (The M.I.T. Press, Cambridge, Mass., 1964), p. 51.
5. A. J. Turski, Nuovo cimento, Vol. 63B, No. 1, p. 115, 1969.

XIV. PLASMAS AND CONTROLLED NUCLEAR FUSION*

B. Diffusion and Turbulence

Academic Research Staff

Prof. T. H. Dupree
Prof. L. M. Lidsky

Graduate Students

K. R. S. Chen
H. R. Greenberg
P. M. Margosian
G. K. McCormick
G. D. Pine
L. C. Pittenger
A. E. Wright

RESEARCH OBJECTIVES

1. Differential Cross-Section Measurements

Techniques developed in magnetic-mirror experiments can be applied to the rapid and accurate measurement of differential scattering cross sections. The main feature in this experiment is the use of the mirror fields, rather than slits or edges, as angle-discriminating elements. The result is the ability to use the total azimuthally integrated scattering from a line source as the scattering signal, thereby improving both sensitivity and the signal-to-noise ratio. Differential scattering cross sections have been measured for argon, helium, neon, and nitrogen. The results are in good accord with published values except for angles greater than 80°. We understand the reason for this discrepancy and are attempting to resolve it.

L. C. Pittenger, L. M. Lidsky

2. Toroidal Electron Trap

Our original experiment for measuring the lifetime of electrons circulating in a toroidal magnetic trap has been completed. The technology needed to inject electrons into the trap and to measure their lifetime has been perfected. A sweeping system to permit measurement of the angular distribution of the circulating electrons has been built and is being tested. This apparatus will be used for the study of waves propagating on electron beams and as a test bed for some experiments to be done on Alcator. To this end, we have designed an electrode structure to give us a phase-stabilized beam. This will be used for the accurate mapping of flux surfaces.

P. M. Margosian, L. M. Lidsky

3. Incoherent Scattering – Anisotropic Velocity Distribution

We plan to use incoherent scattering techniques to measure the distribution of plasma electron velocities in the directions parallel and perpendicular to the confining magnetic field. Experiments show that the electron temperature in the HCD plasma is anisotropic and that the degree of anisotropy depends on several plasma

*This work is supported by the U.S. Atomic Energy Commission (Contract AT(30-1)-3980).

parameters. Our first aim is to determine whether thermalization is caused by classical (Coulomb) scattering or by wave-particle interactions. A hollow-cathode arc plasma source has been built specifically for this experiment with greater than usual emphasis placed on diagnostic access. A 100-MW Q-switched laser has been provided and tested.

G. K. McCormick, L. M. Lidsky

4. Coherent Scattering from Steady-State Plasmas

We are attempting to observe coherent scattering of 10.6 μ radiation from the moderate density steady-state plasma produced by the hollow-cathode discharge source. Our goal is the comparison of the experimentally measured and theoretically predicted scattered spectra in order to determine the spectrum of plasma density fluctuations, that is, to measure plasma turbulence. We are using a 100-W N_2-CO_2He laser as a radiation source and cryogenic Ge detectors.

Measurements of signal-to-noise ratios for the separate parts of this system have been completed. It appears that final S/N ratios of 6 are achievable. We hope to observe the detailed structure of the plasma-frequency satellites.

K. R. S. Chen, L. M. Lidsky

5. Superconducting Magnet Design Studies

It is clear that high-field steady-state plasma confinement experiments will require the use of superconducting coils. We are studying the applicability of superconductor technology to various toroidal plasma systems. We are studying, in particular, the design problems of a 100-kG neutral ion-injected Tokamak experiment and of a uniconductor high-shear stellarator. In order to gain direct experience working with modern superconducting materials, we have constructed a single low-field element of a possible linear quadrupole pair.

A. E. Wright, L. M. Lidsky

1. SUPERCONDUCTING QUADRUPOLE MAGNET

Introduction

A facility for experimental studies of the basic behavior of magnetically confined hot plasmas is under construction for cooperative use by the Departments of Nuclear Engineering, Physics, and Electrical Engineering, M.I.T. The machine is a linear quadrupole, a subset of a general class in which the magnetic confining fields are created by pairs of bars carrying high currents in the same direction and sense. The nature of the field is such that the confined plasma surrounds the current bars.

The array of parallel bars may be either linear or toroidal in shape. Linear multipoles afford a simplicity of magnetic field shape not possessed by toroidal multipoles, thereby allowing easier interpretation and understanding of plasma behavior both experimentally and theoretically. On the other hand, linear multipoles have ends through which plasma may be lost. Such loss has been shown to be not critical, being in fact less than that due to radial diffusion of the plasma to the walls.

A number of multipole machines are, at present, operating at several other laboratories. These are generally of the quadrupole (two current bars) or octopole (four current bars) type existing in both the linear and toroidal versions and in a wide range of sizes. In the case of a linear multipole, a minimum of technical complexity affords a great deal of knowledge of plasma behavior, much of which has yet to be obtained from such a device. Such knowledge has application to the plasmas generated in machines such as stabilized mirrors and Tokamaks wherein similar plasma particle behavior is found.

Normal vs Superconducting Windings

With the attainment of high reliability and low cost in superconducting wire it has become necessary in the design of large magnets to consider the relative advantages and disadvantages of superconducting vs normally conducting windings. Factors in such a consideration relevant to the magnet of a linear quadrupole machine operating in the facilities available to the Research Laboratory of Electronics are the following. The power requirement of normally conducting magnets with the desired current (100 kA per bar) necessitates operation at the Francis Bitter National Magnet Laboratory. Even there, however, such power is available only periodically because of the necessity of sharing the Laboratory's power capacity with other experiments. Thus there is a twofold lack of convenience in both location and availability. Also, with the large water-flow rate that is required to cool the copper current bars, a space-consuming array of pipes and current return lines is encountered.

A superconducting winding circumvents these problems, but provides some of its own. There is increased difficulty at the design stage because of the cooling maintenance of a large massive body at 4.2°K and the marked changes in physical properties among materials relative to their room-temperature values. The main operating cost of the superconducting coil is accountable to liquid-helium consumption and requires careful minimization of heat-transfer rate during design. Minimization of the resulting liquid-helium consumption may well result in a sufficiently low operating cost that would be even more economical than the use of a copper coil, with the choice of location and continuous availability as bonuses.

To members of the Plasma Physics Group of the Department of Nuclear Engineering, M.I.T., superconducting coils for the linear quadrupole have the additional advantage of providing an opportunity for students to develop expertise in cryogenics and superconducting magnet design and operation.

Characteristics of the Superconducting Quadrupole Magnet

We decided at the outset that constructing a full-scale test magnet possessing most of the characteristics of the desired final design would be an effective means of testing

the efficiency of the cryostat and providing an extreme test of behavior of the superconducting wire. In the mock-up planned, only several turns of the superconductor would be needed; thus the considerable cost of the full superconducting windings would be avoided.

This wire would be placed, however, in a more restrictive environment than would be allowed in the final version, thereby testing its margin of reliable operation. The cryostat would be designed for easy disassembly, and hence be available for use in the construction of the final magnet version.

Choosing 200 A as a convenient operating current leads to 500 turns of 0.021 in. diameter superconducting wire to provide the 10^5 ampere-turns required for the linear quadrupole. The wire selected has 121 strands of NbTi embedded in a copper matrix with a 3:1 ratio of copper to superconductor. The entire matrix is twisted two turns per inch for increased stability. Such wire is said to be stable at currents closely approaching its critical current, even when wound without spacers. To provide a test of this prediction, the test magnet was wound with 1500 turns of 0.021 in. diameter insulated copper wire, which resulted in an approximately 1 inch square winding cross section. At the center of this cross section three turns of the superconducting wire were wound electrically independent of the copper windings. The winding of the final magnet version, containing 500 turns of 0.021 in. diameter superconducting wire only, is thereby simulated, except that the 1000 extra turns will further limit the flow of liquid helium to the winding center. This provides an abnormally severe test for the superconducting wire at the center.

The magnet is toroidal in shape with essentially rectangular major and minor cross sections, dimensions of the former being 1.5 × 1 m, and the latter approximately 5 × 6 cm (Figs. XIV-9 and XIV-10). The linear quadrupole machine will require two such magnets with a longer leg of each providing one of the pair of parallel current bars (Fig. XIV-11). The minimum desired bar separation is 20 cm, yielding a maximum attractive force between the 4.2°K bars of approximately 2200 lbs (9800 N) per meter. This force must be supported at 4.2°K to keep the heat-transfer rate to the bars low. If it were transmitted instead to a 77°K or room-temperature structure through a sufficiently strong support, large heat-transfer rates or very long supports would result. The practical solution is shown in Fig. XIV-11 where the adjacent magnet legs are separated by short stainless-steel members. A liquid nitrogen-cooled radiation shield prevents 300°K radiation from the vacuum vessel walls from reaching the magnet bars.

The designer is faced with three conflicting problems: (i) minimizing the degree of magnet bending, hence the axial magnetic field variation, (ii) minimizing the magnet cross-sectional area, hence maximizing the plasma containment volume, and (iii) providing sufficient space within the magnet for the windings and flow of liquid

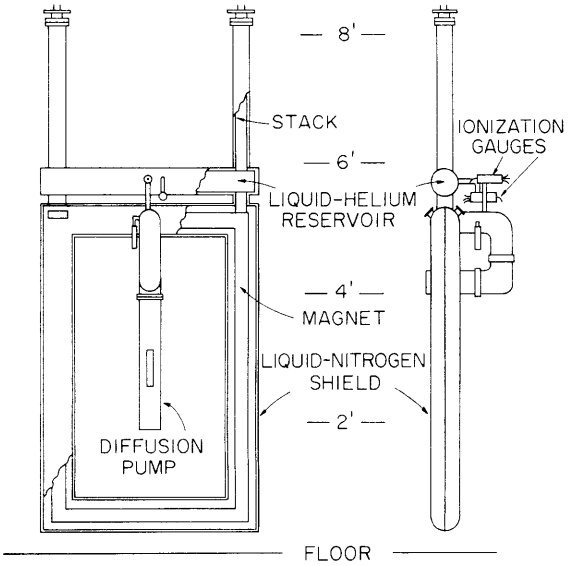

Fig. XIV-9.
Over-all view of test magnet assembly.

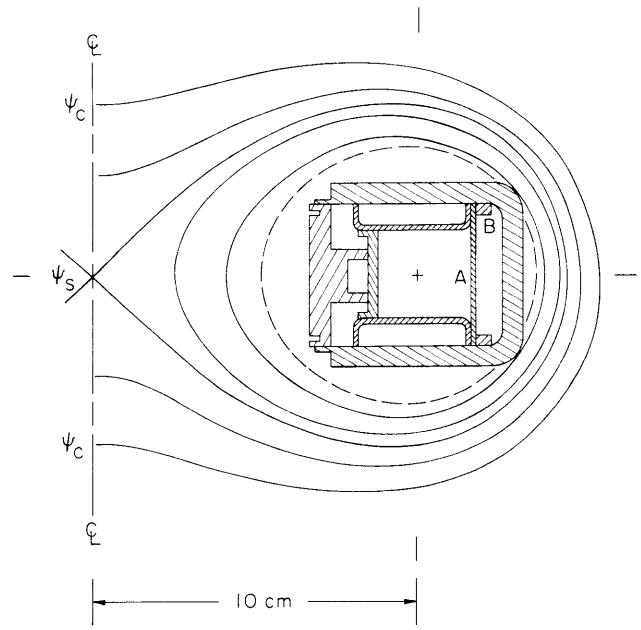

Fig. XIV-10.
Quadrupole magnetic field plot with the location of the magnet (shown in cross section). The cross indicates the winding center.

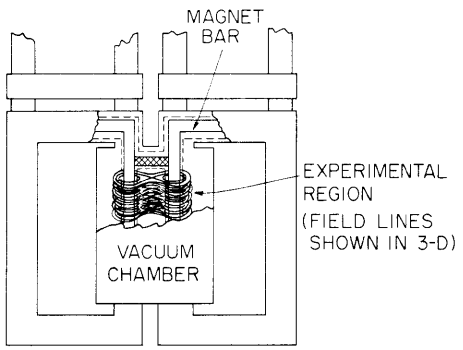

Fig. XIV-11.
Quadrupole magnet pair situated in a vacuum chamber for plasma experiments. The supporting member is shown crosshatched. Dashed lines indicate heat shields.

helium. A simple adequate solution is shown in Fig. XIV-10, where the magnet's minor cross section is shown in full scale within the magnetic field configuration. The magnet is built of 1/4 in. 304 stainless-steel flat stock bent into box-channel shape. Four T-shaped covers are welded to the channel to form a vacuum-tight high-strength enclosure for the windings and liquid helium. The square winding volume is located in the center of the magnet cross section, the wire being supported by perforated teflon-coated stainless-steel plates. Liquid helium is allowed to circulate freely around the winding volume. Circulation within the windings is determined by the size and tightness of winding of the wire.

Because of the difference in thermal conductivity between the copper wire and stainless-steel container, there will be a different rate of cooling, hence thermal contraction, of the two during cooling down. Unless this is limited the yield stress of the wire will be exceeded. This was avoided by terminating the supports B in Fig. XIV-10 a distance of 4 cm from the ends of the magnet legs, thereby allowing the perforated plate A to cantilever the remaining distance. The deflection of the cantilever by the tensile force developed in the wire during cooling down is sufficient to limit that force to a safe value.

The magnet is surrounded by a vacuum-tight copper shell shown in Fig. XIV-9 which will be cooled to 77°K by liquid nitrogen. The liquid-nitrogen jacket and thermal insulation have been omitted for clarity. The annular region between the magnet and liquid-nitrogen shell will be highly evacuated by a baffled diffusion pump and by its own cryopumping. The principal means of heat transfer to the 4.2°K magnet is via conduction through the tubular stacks serving both to support the magnet within the dewar and to vent the helium vapor. The expected liquid-helium loss rate of the dewar is 0.3 liter per hour.

A. E. Wright

XIV. PLASMAS AND CONTROLLED NUCLEAR FUSION*

C. Plasma Diagnostics

Academic and Research Staff

Prof. G. Bekefi
Prof. E. V. George
Dr. P. A. Politzer

RESEARCH OBJECTIVES

The aims of this group are to perfect and refine existing methods of studying the properties of plasmas and, in particular, to devise novel techniques. At present, we are concentrating on the effects of intense high-frequency electric fields acting on excited atoms. Under suitable conditions these fields can give rise to quantum transitions that are normally forbidden by standard selection rules. At present, we are using these techniques to study the spatial and temporal density distributions of laser-produced plasmas, using a high-power CO_2 laser as the source.

G. Bekefi

1. OPTICAL SATELLITES INDUCED IN A PLASMA THROUGH THE ACTION OF INTENSE, HIGH-FREQUENCY ELECTRIC FIELDS

We have been making a spectroscopic study of a laser-produced plasma. To produce a more uniform plasma at breakdown, we have modified our CO_2 laser in the following manner. Now the laser comprises a series of resistors, the legs of which act as anodes, spaced in a helical pattern on 2" O.D. Plexiglas tubing, 1.5 m long. Diametrically opposite each resistor leg is placed a pin cathode. The excitation scheme involves charging a 0.03 μF capacitor to 25 kV and then discharging it through the laser tube via a hydrogen thyratron.

This laser produces ~1-2 MW laser pulses of ~200 ns width at a repetition rate of 10 pps. The optimum operating pressure is 320 Torr. The high repetition rate and good shot-to-shot reproducibility of this laser allowed us to make spatial and temporal studies of our plasma with good signal-to-noise ratios by means of standard boxcar integration techniques.

As before,[1] the laser radiation is focused by means of a 3.8 cm focal length germanium lens either into a cell containing ~1 atm of spectroscopically pure helium, or onto a cylindrical metallic post of lithium. The post is continually rotated so as to minimize pitting of the metallic surface by the laser.

*This work was supported by the U.S. Atomic Energy Commission (Contract AT(30-1)-3980).

The experimental arrangement was illustrated in a previous report.[1] The light from the plasma is focused onto the slits of the 0.5 m scanning spectrometer. The output from the spectrometer was fed into the boxcar integrator and graphic display equipment. The boxcar gate width is typically 250 ns and thus represents the time resolution of our measurements.

The germanium laser focusing lens and gas cell is mounted on a vernier carriage so that lateral scanning of the plasma is also possible. The spatial resolution is approximately 0.1 mm.

Figure XIV-12 illustrates the Stark-broadened spectrum of the neutral He 5876 Å line, at a time ~10 μs in the afterglow. The dots are a computer profile fit of the data following the method outlined by Griem.[2] It is evident that the best fit is obtained

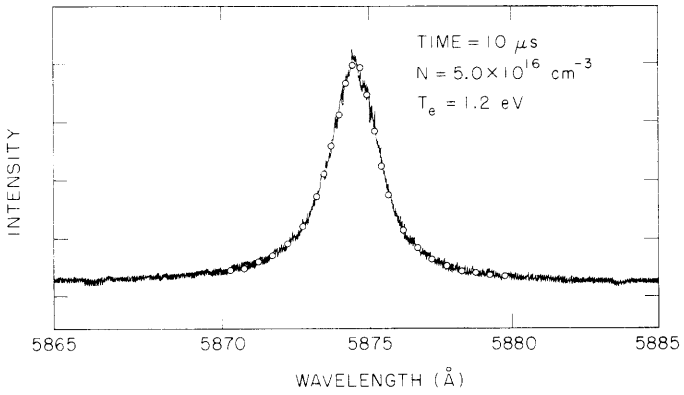

Fig. XIV-12. Stark-broadened spectrum of the neutral He 5876 Å line. The dots are a theoretical profile fit of the experimental data.

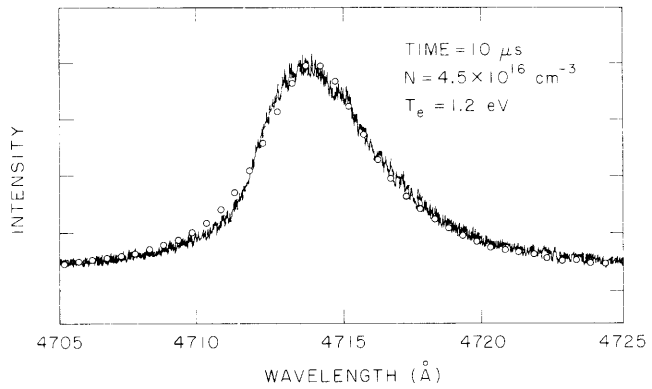

Fig. XIV-13. Stark-broadened spectrum of the neutral He 4713 Å line. The dots are a theoretical profile fit of the experimental data.

for a density of 5×10^{16} cm^{-3} and an electron temperature of 1.2 eV. Figure XIV-13 illustrates the spectrum of the neutral He 4713 Å line under identical conditions. Note that the best fit corresponds to approximately the same density and temperature as in Fig. XIV-12. The excellent agreement between measured and calculated profiles gives us confidence that we are justified in using Stark broadening as an accurate density probe of our plasma.

One of the observed visual characteristics of this CO_2 laser-produced plasma is that the plasma appears to consist of a very intense inner core a few tenths of a mm in diameter by a few mm in length surrounded by a much less intense larger halo. This is reflected in the spectroscopic measurements of the Stark widths of the ionized and neutral He lines; there is good agreement between the electron densities obtained by using the Stark widths of various neutral lines but the density obtained by using the Stark width of the ion line is always larger. We thus concluded that the ion lines emanate predominantly from the intense inner core, while the neutral lines come, for the most part, from the less intense outer halo.

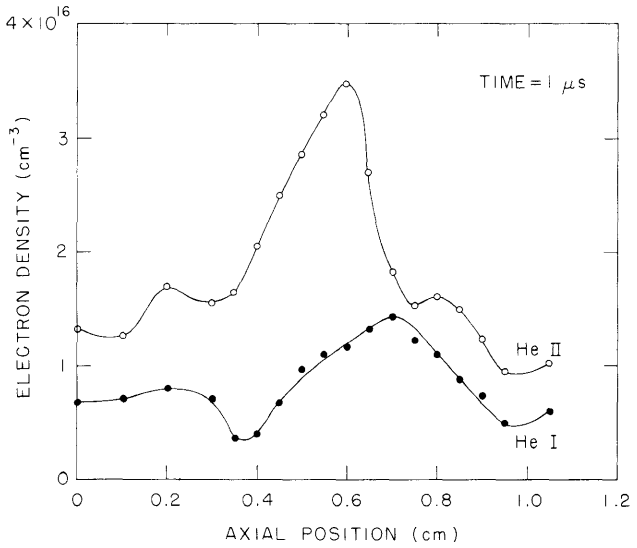

Fig. XIV-14. Spatial dependence of the electron density as obtained from the Stark widths of the neutral He I (5876 Å) line and the ion He II (4686 Å) line, at a time 1 μs in the afterglow.

In Fig. XIV-14 we illustrate the spatial dependence of the electron density as obtained from the Stark widths of the neutral He I lines and of the ion He II lines at a time 1 μs in the afterglow. The germanium laser focusing lens is toward the right-hand side of this figure. At this time, in the afterglow, the sizes of the

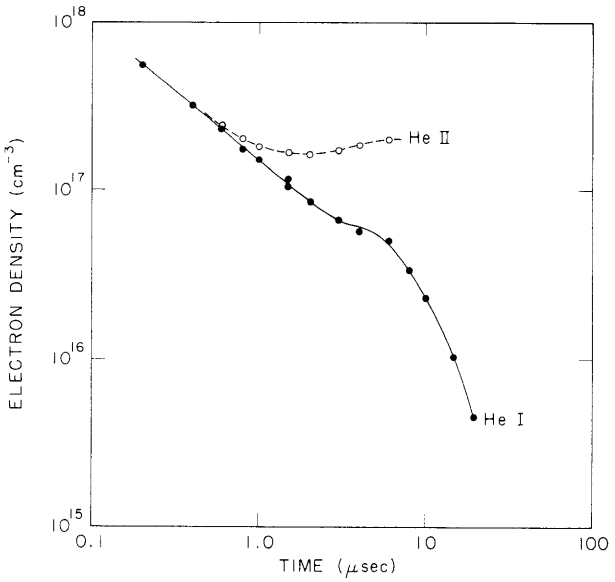

Fig. XIV-15. Time dependence of the electron density as obtained from the Stark widths of the He I and He II lines. Here the boxcar gate width was 250 ns.

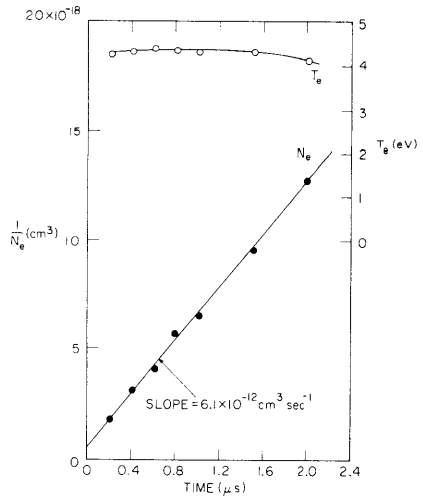

Fig. XIV-16. Lower curve is the reciprocal of electron density as obtained from Fig. XIV-15 as a function of time. Upper curve is electron temperature as a function of time.

two plasmas are approximately 0.5 cm, the outer halo being somewhat broader than the inner core. Similar measurements made at later times show a much stronger distinction between the two regions; the outer halo is much larger than the inner core. The apparent increase in density at these points is thought to be due to reflections of light from the back wall of the cell entering the spectrometer slits. We are now in the process of constructing an Abel transform of our results in order to obtain a true spatial density profile. This transformation has not been made on the data shown here.

In Fig. XIV-15 we illustrate the time dependence of the electron density as obtained from the Stark widths of the neutral and the ion spectral lines. We see that at very early times the two densities are equal, but soon significant departures occur, thereby indicating that the separation into a hot core and a halo occurs at ~0.5 μs in the afterglow. It is noteworthy that the two plasmas decay at different rates. Indeed the hot core shows a slight increase in density around 6 μs. We feel that the formation of this outer halo is possibly due to the blast wave that carries plasma out of the initial breakdown region and produces additional ionization at the shock front.

Using our spectroscopic techniques, we have measured the expansion rate of the halo and found that it is proportional to $t^{0.3}$, as compared with blast wave theory which yields an expansion rate proportional to $t^{0.4}$. Using the density data of Fig. XIV-15, we plot the reciprocal of density as a function of time as shown in Fig. XIV-16. The straight line and value of the slope is suggestive that collisional-radiative recombination is the major plasma loss mechanism. The slope is in good agreement with the theoretical results of Mewe[2] and Bates et al.[3]

The electron temperature is seen to be almost constant over this period of time. These values were obtained in the usual way by measuring the ratio of intensities of an ionized and a neutral helium line. In our case, however, this technique is highly suspect because the two radiations come from different regions, the core and the halo. Hence this temperature is at best some average temperature.

One of the major difficulties in using Stark broadening as a diagnostic probe of electron density for high-density plasmas is the phenomenon of self-absorption. At high densities the radiation emitted from the center of the plasma is absorbed by the less dense cooler outer regions of the plasma. The spectral line, when wavelength-scanned, is self-reversed at and near line center; hence, determination of an accurate linewidth is extremely difficult. The degree of self-absorption is determined primarily by the oscillator strength and the degeneracy of the line (e.g., a triplet suffers more self-absorption than a singlet). We have been studying weak forbidden transitions for use as a measure of the electron density.

Such forbidden transitions occur because of so-called level mixing of the allowed

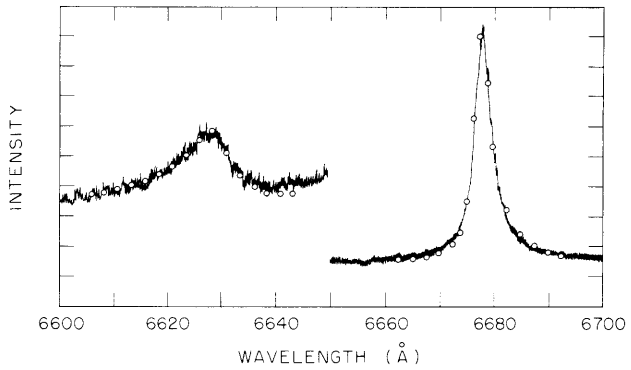

Fig. XIV-17. Spectrum of the triplet He I 4471 Å allowed line and the 4469 Å and 4523 Å forbidden lines. The dots are a theoretical profile fit of the experimental data.

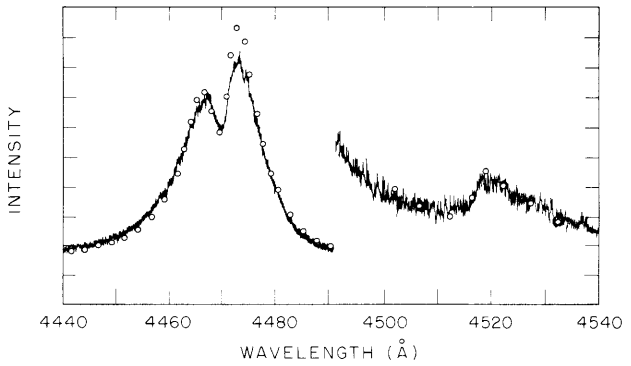

Fig. XIV-18. Spectrum of the singlet He I 6678 Å allowed and 6634 Å forbidden lines. The dots are a theoretical profile fit of the experimental data.

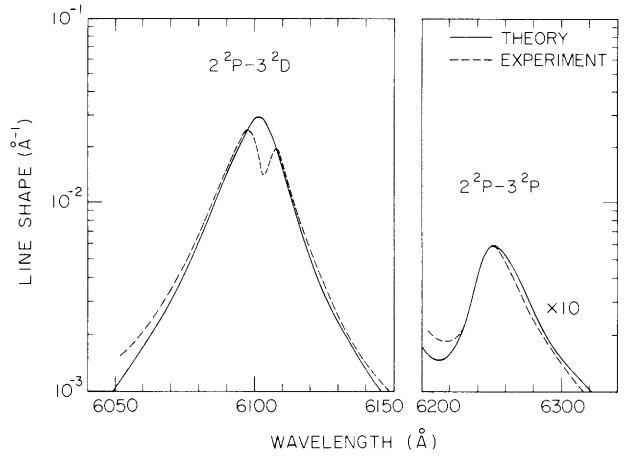

Fig. XIV-19. The spectrum of the Li I, 6103 Å allowed and 6240 Å forbidden lines. Notice the strong self-absorption of the allowed line.

and forbidden lines. This can be theoretically treated by considering the total wave function to be a linear combination of the upper levels of the forbidden and allowed lines. These coefficients are a function of the local electric fields, and are obtained by considering the ions to be stationary, and the electrons are treated by using the so-called impact approximation.

In general, to verify the theory, we determine the density using lines that suffer little self-absorption (in He, for example, we used the lines illustrated in Figs. XIV-12 and XIV-13). The comparison between the theoretical and experimental profiles of various He and Li forbidden lines is illustrated in Figs. XIV-17 through XIV-19. Notice that the lithium allowed line (shown in Fig. XIV-19) shows strong evidence of self-absorption.

E. V. George, G. Bekefi, R. J. Hawryluk, B. Ya'akobi

(Dr. B. Ya'akobi is a member of the Department of Physics and Astronomy, University of Maryland.)

References

1. E. V. George, M. Pawlak, and G. Bekefi, Quarterly Progress Report No. 98, Research Laboratory of Electronics, M.I.T., July 15, 1970, pp. 53-55.
2. H. R. Griem, Plasma Spectroscopy (McGraw-Hill Book Company, New York, 1964).
3. R. Mewe, Brit. J. Appl. Phys. 18, 107 (1967).
4. D. R. Bates, et al., Proc. Roy. Soc. (London) 267A, 297-312 (1962).

XIV. PLASMAS AND CONTROLLED NUCLEAR FUSION*

D. Fusion-Related Studies

Academic Research Staff

Prof. L. M. Lidsky
Prof. R. A. Blanken
Prof. R. J. Briggs

Graduate Students

R. L. McCrory

RESEARCH OBJECTIVES

1. Fusion Feasibility

We will continue our work on the analysis of fusion power systems with particular emphasis given to the possibilities inherent in fission-fusion symbiosis. The combination of marginal D-T fusion reactor with an MSCR fission reactor operating on the thorium cycle will be analyzed in more detail. Another system to be studied during the next year is the D-D cycle mirror reactor with direct conversion. It appears that efficient use of the neutrons generated in the complete D-D cycle may suffice to make this concept economically viable also.

L. M. Lidsky

2. Economics of Reactor Concepts

All known fusion reactor concepts contain some difficult physical questions that are often overlooked in the simple economic analyses done thus far. We plan to analyze several of the more important of these to see their effect on fusion reactor economics. For example, there is considerable experimental and theoretical evidence that the maximum allowable β in toroidal systems will be a strong function of the aspect ratio. Studies of the economics of toroidal reactors are being undertaken using realistic assumptions for the functional dependences of β on the aspect ratio. For another example, the crucial problems of synchrotron radiation have been handled very approximately in previous studies. A re-examination of the economics of mirror reactors using more realistic models for radiation reabsorption is under way.

R. A. Blanken

*This work is supported by the U.S. Atomic Energy Commission (Contract AT(30-1)-3980).

XIV. PLASMAS AND CONTROLLED NUCLEAR FUSION*

E. Feedback Stabilization

Academic Research Staff

Prof. R. R. Parker
Prof. K. I. Thomassen

Graduate Students

R. K. Linford
R. S. Lowder
A. R. Millner

RESEARCH OBJECTIVES

The objectives of this research are to use feedback control techniques for the diagnostic study and suppression of instabilities in plasmas. Under investigation are ways to couple the feedback system to the plasma, the applicability of this method to fusion devices, and the study of continuum feedback methods in general.

Present studies include investigations of the drift instability in a moderately energetic plasma (10^{12} density, 15 eV temperature) and ways to couple to it, MHD instabilities in a Tokamak and coupling schemes for their suppression, and adaptation of the methods of modern control theory to the general problem of continuum feedback control.

R. R. Parker, K. I. Thomassen

*This work is supported by the U.S. Atomic Energy Commission (Contract AT(30-1)-3980).

XIV. PLASMAS AND CONTROLLED NUCLEAR FUSION*

F. High-Temperature Toroidal Plasmas

Academic and Research Staff

Prof. B. Coppi
Dr. D. B. Montgomery†
Prof. G. Bekefi
Prof. A. Bers
Prof. R. A. Blanken
Prof. R. J. Briggs
Prof. L. M. Lidsky
Prof. R. R. Parker
Prof. K. I. Thomassen
Dr. U. Daybelge
Dr. R. Gajewski
Dr. P. A. Politzer

Graduate Students

E. L. Bernstein
R. Dagazian
D. P. Hutchinson
Y. Y. Lau
M. A. Lecomte
A. R. Milner
M. Simonutti
E. N. Spithas
B. V. Waddell
D. C. Watson

RESEARCH OBJECTIVES

The physics of high-temperature plasmas is of primary importance in the problem of controlled thermonuclear fusion and to astrophysics in general. The main point of interest for the controlled thermonuclear program is the production and magnetic confinement of dense plasmas ($n \gtrsim 10^{14}$ particles/cm^3) with thermal energies in excess of 5 keV. One of the most debated questions in astrophysics, at present, is the nature of thermal and nonthermal radiation mechanisms from the magnetosphere of collapsed stars (X stars and pulsars are thought to belong to this class).

Considerable experimental and theoretical effort has been undertaken in order to understand the dynamics of plasmas in the regimes mentioned above, and in particular their transport properties. In fact, it is recognized that in conditions wherein the two-body collision mean-free paths are very long the transport coefficients of a plasma are determined, for the most part, by the collective modes that are excited in it rather than by two-body collisions.

In magnetically confined plasmas at high temperatures two classes of particles may be distinguished: particles that are trapped in the local wells of the inhomogeneous magnetic field and circulating particles that sample the entire length of the lines of force. As a result, new collective modes can be generated and have an important effect on the stability and transport properties of the plasma that is being considered.

To investigate these and other aspects, a sequence of experimental apparatus is being put into operation: a linear quadrupole that is the simplest two-dimensional configuration for the study of trapped-particle dynamics, a small toroidal configuration (Minitor) to study the effect of turbulent resistivity and plasma microwave heating, a relatively large toroidal configuration (Alcator) designed to achieve new plasma regimes and to analyze new methods of plasma heating.

A special experimental program is being organized to investigate the x-ray, optical, and infrared emission from Alcator. This is in view of its astrophysical implications and of the importance that radiation has in the energetic balance of thermonuclear plasmas.

B. Coppi

---

*This work was supported by the U.S. Atomic Energy Commission (Contract AT(30-1)-3980).

†Dr. D. Bruce Montgomery is at the Francis Bitter National Magnet Laboratory.

1. DENSITY EXPANSION OF THE EXACT MASTER EQUATION

The purpose of this report is to give a direct method for obtaining the density expantion of the exact master equation given by Zwanzig.[1] Expansion of the same equation in the interaction strength leading to the Fokker-Planck type of equations has already been discussed by Zwanzig[1] and by Muriel and Dresden.[2] Such expansions are not directly applicable, however, to many physical systems, including molecules with hard-core potentials and plasmas. For such systems, one must first resort to complicated resummation procedures to all orders in the density.[3] The method presented here for the direct density expansion is analogous to the inner expansion techniques used in fluid mechanics.[4]

We start with the exact master equation for the N-particle momentum distribution function[1] written in the form

$$\frac{\partial}{\partial t} Pf_N(t) = -i \int_0^t \frac{\partial}{\partial y} H_N(y)\, Pf_N(t-y)\, dy, \tag{1}$$

where

$$H_N(y) = PL \exp -iy(1-P)\, L$$

$$P = V^{-N} \int d\underset{\sim}{r}_1 \cdots d\underset{\sim}{r}_N$$

$$L = L_o + \lambda L_1 = -i \sum_j \frac{\underset{\sim}{p}_j}{m} \frac{\partial}{\partial \underset{\sim}{r}_j} + i\lambda \sum_{1 \le j < k \le N} \frac{\partial V_{jk}}{\partial \underset{\sim}{r}_{jk}} \left(\frac{\partial}{\partial \underset{\sim}{p}_j} - \frac{\partial}{\partial \underset{\sim}{p}_k} \right),$$

with $\underset{\sim}{r}_{jk} = \underset{\sim}{r}_j - \underset{\sim}{r}_k$. The underlying assumption in (1) is that initially f_N is independent of particle positions. Here, λ denotes the interaction strength, and $V_{kl}(r_{kl})$ is a power-law potential, $V_{kl} = \lambda r_{kl}^{-\alpha}$, where $\alpha > 0$.

In near collisions, the distance between particles can be so small that interaction with other particles may be neglected. To indicate such close separations let us introduce new magnified relative coordinates[4]

$$\underset{\sim}{R}_{kl} = \lambda^{-1/(1+\alpha)} \underset{\sim}{r}_{kl}. \tag{2}$$

If (2) is substituted in the Liouville operator L, it yields

$$L = L_o + i \frac{\partial V_{kl}}{\partial \underset{\sim}{R}_{kl}} \left(\frac{\partial}{\partial \underset{\sim}{p}_k} - \frac{\partial}{\partial \underset{\sim}{p}_l} \right) + 0(\lambda). \tag{3}$$

By neglecting terms of order λ, (3) represents the binary collision approximation of the Liouville operator $L = L_o + L_{kl}$. Similarly, we can consider n-body collisions. Let I_n denote the set of indices of n particles, so that $2 \leq n$ and $I_n \subset \{N\}$. Also, let J_n denote the set of binary subsets of I_n. Then J_n contains $n(n+1)/2$ pairs of indices α_k. Introducing new magnified coordinates $\underset{\sim}{R}_{\alpha_k}$ for each pair α_k as indicated in (2), we find

$$L = L_o + \sum_{\alpha_k \in J_n} L_{\alpha_k} + 0(\lambda). \tag{4}$$

The corresponding n-body operator H_n may lead to all s-ary collisions among s particles, where $s \leq n$. Therefore, a new operator, $B_{n-1}(I_n)$, can be defined recursively as

$$B_{n-1}(I_n) = H_n - \sum_{s=1}^{n-2} \sum_{I_{s+1} \subset I_n} B_s(I_{s+1}). \tag{5}$$

Clearly, $B_{n-1}(I_n)$ is a true (irreducible) n-body collision operator. Reciprocally, the operator H_N can be expressed from (5), by generalizing it for n = N. Substituting H_N in (1), we obtain

$$\frac{\partial}{\partial t} \Phi_N(t) = -i \int_0^t \frac{\partial}{\partial y} \sum_{s=1}^{N-1} B_s(y)\, \Phi_N(t-y)\, dy, \tag{6}$$

where

$$\Phi_N = Pf_N$$

and

$$B_s(y) = \sum_{I_{s+1} \subset \{N\}} B_s(I_{s+1}).$$

It is important to note that in the derivation of (6) no assumptions have been made about the number of particles or the containing volume. Defining the density as $c = N/V$ when when $N, V \to \infty$, we note that the B_s are proportional to c^s. In a detailed report on this and other results for plasmas we have shown that the use of the approximation[5] $H_N(y) = PL \exp -itL$ in connection with the above-mentioned method leads to Weinstock's master equation.[6]

U. Daybelge

References

1. R. Zwanzig, Boulder Lectures in Theoretical Physics, Vol. III (Interscience Publishers, Inc., New York, 1961).

2. A. Muriel and M. Dresden, Physica 43, 424 (1969).

3. T. Y. Wu, Kinetic Equations of Gases and Plasmas (Addison-Wesley Publishing Company, Reading, Mass., 1966).

4. M. Van Dyke, Perturbation Methods in Fluid Mechanics (Academic Press, New York and London, 1964).

5. U. Daybelge (unpublished).

6. J. Weinstock, Phys. Rev. 132, 454 (1963).